RSC Advances

ROYAL SOCIETY OF CHEMISTRY

www.rsc.org/advances

Facile electrochemical assisted synthesis of ZnO/graphene nanosheets with enhanced photocatalytic activity

Sandesh Y. Sawant and Moo Hwan Cho*

School of Chemical Engineering, Yeungnam University,

Gyeongsan-si, Gyeongbuk 712-749, South Korea.

E-mail: mhcho@ynu.ac.kr; Fax: +82-53-810-4631; Tel: +82-53-810-2517

Abstract

In the present study, an electrochemical exfoliation technique was used to synthesize a series of zinc oxide/graphene (ZnO/Gr) nanocomposites using different concentrations of zinc nitrate in an electrolyte solution. The prepared ZnO/Gr nanocomposites were characterized using a range of analytical techniques and evaluated further for their photocatalytic activity over methyl orange (MO) and rhodamine B (RhB) under UV light. Scanning electron microscopy and transmission electron microscopy showed that the ZnO/Gr nanocomposite synthesized using 7 mmol of zinc nitrate exhibited a sheet-like morphology with a uniform decoration of ZnO nanoparticles over the graphene sheets, as well as the maximum photodegradation capacity for MO (> 96%) and RhB (> 89%) among the composites prepared. The loading of graphene was found to be crucial for deciding the enhancement in the photocatalytic activity, and resulted in a remarkable improvement in photocatalytic activity (~ 7 times for MO and ~ 2 times for RhB) over bare ZnO. Photoluminescence spectroscopic analysis revealed the improved separation of electron-hole pairs with the graphene loading, which is mainly responsible for the enhanced

photocatalytic activity. The present work possesses the advantage of *in-situ* synthesis of few layered less defective graphene/ZnO composite with enhanced photocatalytic activity.

Keywords: Photocatalyst; ZnO nanoparticles; Methyl orange; Rhodamine B; UV light; Electrochemical exfoliation

1. Introduction

The remediation of water pollution using heterogeneous semiconductor photocatalysts, such as zinc oxide (ZnO), TiO_2 and CeO_2, has been investigated extensively.[1-3] Several other applications of photocatalysts, such as water splitting,[4] photocatalytic reduction,[5] and selective organic transformations[6] have also been reported. Among the various semiconductor materials, ZnO, with a wide band gap of 3.37 eV and a large excitation binding energy of ~60 meV, has attracted considerable interest as a photocatalyst due to its higher photocatalytic efficiency for liquid-phase degradation and stability.[7] The photodegradation efficiency of the photocatalysts is dependent mainly on (i) the effective transference of photoelectrons with significantly impede the recombination of photoelectrons and holes, (ii) a better absorption capacity of the catalytic system toward the dye or pollutants and (iii) a proper substrate as a scaffold to immobilize and support the catalyst. In recent years, several structural modifications, such as metal doping,[8] coupling with other metal oxides,[9] creating oxygen vacancies,[10] and combining with carbonaceous materials, have been reported to enhance the photocatalytic activity and stability of ZnO.

ZnO composites with different carbonaceous materials, including fullerene,[11] carbon nanotubes,[12] graphite,[13] graphene,[14] and porous carbon[15] showed the significant enhancement in

their photocatalytic activity and stability, due mainly to the increased surface area with higher adsorption and prolonged recombination effect of photoelectrons and holes. Graphene, which is an individual sheet of graphite with a hexagonal two dimensional network of sp^2- hybridized carbon atoms having ~ 1 nm thickness, has been assessed as a constituent material for a range of composites owing to its excellent mechanical and electrical properties. Recently, Chen et al.[16] reported that ZnO nanorod composites with graphene exhibited higher photocatalytic activity than bare ZnO nanorods because of the integrative synergistic effects of enhanced adsorption capacity and the improved lifetime of photogenerated electron–hole pairs.

Various methodologies, including hydrothermal,[17] solvothermal,[18] chemical vapor deposition,[19] and electrochemical[20] have been reported for the synthesis of zinc oxide/graphene (ZnO/Gr) composites with different morphologies. Gong et al.[21] reported the synthesis of rose-like ZnO/reduced graphene oxide composite under reflux conditions. In most of the synthesis routes, graphene or graphene oxide had been prepared using the modified Hummer's method. The electrochemical exfoliation of graphite is a promising alternative approach for obtaining high quality graphene sheets.[22, 23] This paper reports the synthesis of ZnO/Gr nanocomposites via the electrochemical exfoliation of graphite in a zinc nitrate/sulfuric acid electrolyte followed by ZnO formation. In addition, the photocatalytic activity of the obtained ZnO/Gr nanocomposites was investigated by measuring the photodegradation of methyl orange (MO) and rhodamine B (RhB) under UV light.

2. Experimental

2.1 Materials

Zinc nitrate hexahydrate, sulfuric acid and sodium hydroxide were purchased from Duksan chemicals Company, South Korea. The graphite rods used in this study were procured from local suppliers. Methyl orange and rhodamine B were obtained from Sigma Aldrich. All chemicals were used as received.

2.2 Catalyst Preparation

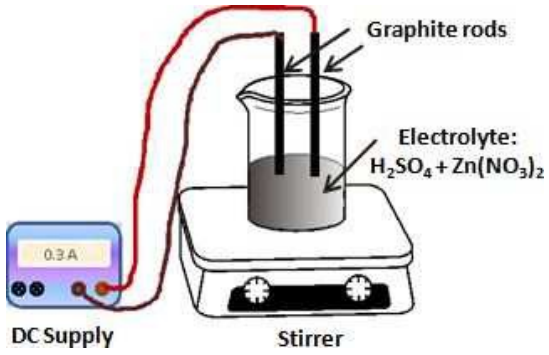

Fig. 1 Electrochemical exfoliation set-up for the synthesis of graphene.

The electrochemical exfoliation technique (Fig. 1) was used for synthesis of graphene using 200 mL of a 0.25 M H_2SO_4 electrolyte containing various concentrations of zinc nitrate hexahydrate (3 to 10 mmol). Two graphite rods were used as the anode and cathode by placing them ~2 cm away from each other and dipped ~2 cm in the electrolyte. A constant current of 0.3 A was supplied for 2 h using a constant DC supply source under stirring. The obtained solution was diluted to 1 L using distilled water and ultrasonicated for 2 h. The larger graphitic particles were separated by centrifuge at 10000 rpm for 30 min. The supernatant solution was ultrasonicated for 2 min before a pH adjustment of ~ 9 using a 10% NaOH solution with stirring. The obtained precipitate was aged at 90 ºC for 2 h followed by filtration and sufficient hot distilled water washing. The $Zn(OH)_2$/Gr composite obtained after drying at 90 ºC for 12 h, was

calcined further at 500 ºC for 1h under nitrogen atmosphere. The obtained ZnO/Gr composite was labeled ZnO/Gr_3, whereas 3 stands for the concentration of zinc nitrate hexahydrate (3 mmol). For a comparative study, the synthesis of bare ZnO was carried out in a similar manner without graphene. The pristine graphene was isolated using the membrane filtration of supernatant solution after centrifugation step followed by sufficient water washing.

2.3 Characterization

The crystallographic phase identification of the samples was characterized by X-ray diffraction (XRD, PANalytical, X'pert PRO-MPD, Netherland) using Cu $K\alpha_1$ (λ = 1.54056 Å) radiation over the 2θ range, 2-80°. Attenuated total reflection – infrared (ATR-IR) and Raman spectroscopy were performed on a Thermo Scientific Nicolet Smart iTR iS10 and HR800 UV Raman microscope (Horiba Jobin-Yvon, France), respectively. The optical properties were examined using a UV-VIS-NIR diffuse reflectance spectrophotometer (VARIAN, Cary 5000, USA) and photoluminescence spectrometry (PL) using a wavelength of 325 nm and power of 50 mW (Kimon, 1 K, Japan), respectively. The morphology of the composite was examined by scanning electron microscopy (SEM, S-4200; Hitachi, Ltd.) and transmission electron microscopy (TEM, JEM-2100 JEOL) with an accelerating voltage of 15 and 200 kV, respectively. The elemental composition of the samples was determined using a CHN/O analyzer (Perkin-Elmer, Optima 8300). Surface area analysis was carried out by nitrogen sorption at 77 K using a Quanta Chrome Autosorb automated gas sorption system (Autosorb-1, Quanta Chrome, USA).

2.4 Photocatalytic activity

The liquid-phase photodegradation of MO and RhB was carried out under the irradiation of UV light. In a typical process, a catalyst (20 mg) was suspended in 50 mL of a 10 ppm dye solution in a 100 mL glass beaker using an ultrasonication treatment for 2 min. The adsorption-desorption equilibrium of the dye on the catalyst was achieved by stirring the suspension in the dark for 30 min. Under ambient conditions and stirring, the solution was exposed to UV irradiation from a UV lamp (16 W; Philips) placed 12 cm above the beaker. A 0.5 mL solution was taken at certain time intervals during the experiments, and centrifuged to remove the catalyst completely. The solution was analyzed on a UV-Vis spectrophotometer (Optizen 2120UV; Mecasys Co., Ltd., South Korea). The percentage degradation is reported as C/C_0, where C is the absorbance of the dye solution after each irradiated time interval at the λ_{max} of the adsorption spectrum (465 nm for MO and 554 nm for RhB) and C_0 is the absorbance of the initial concentration after reaching adsorption–desorption equilibrium.

3. Results and discussion

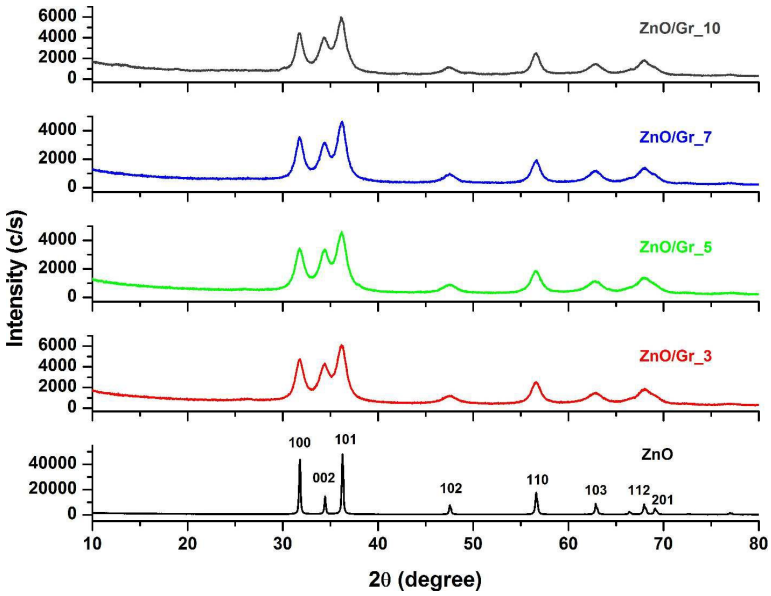

Fig. 2 XRD pattern of the bare ZnO and ZnO/Gr composites prepared with different concentration of the zinc precursor.

The formation and phase identification of the obtained products was confirmed by the powder XRD analysis. The XRD patterns of the bare ZnO and ZnO/Gr composites with different graphene loadings (Fig. 2) exhibited a well resolved peaks, which was indexed to the (100), (002), (101), (102), (110), (103), (112) and (201) planes of the hexagonal structure of ZnO (JCPDS 36-1451).[24] The lack of XRD peaks at 26-27° 2θ belonging to the graphitic 002 planes confirmed the absence of graphitic impurity and the formation of graphene sheets. The crystallite size calculated from the X-ray line broadening of the 100 peak using the Scherrer's equation were 6.8, 7.7, 8.3, 9.2, and 51.0 nm for ZnO/Gr_3, ZnO/Gr_5, ZnO/Gr_7, ZnO/Gr_10, and bare ZnO, respectively. In particular, an increase in the concentration of zinc nitrate during the synthesis process (from ZnO/Gr_3 to ZnO/Gr_10) indirectly implied a decrease in the amount of graphene present in the ZnO/Gr nanocomposites. The loading of the graphene plays a crucial role in the crystallite size of the ZnO/Gr nanocomposite, which increased with decreasing graphene loading. The graphene loading in the ZnO/Gr nanocomposites was calculated from the elemental carbon content determined by CHN analysis. The elemental carbon and hydrogen content (wt.%) of the ZnO/Gr_3, ZnO/Gr_5, ZnO/Gr_7 and ZnO/Gr_10 were 3.72 (C), 0.37 (H); 2.52 (C), 0.38 (H); 1.62 (C), 0.4 (H) and 1.28 (C), 0.50 (H), respectively. The presence of nitrogen was not detected in any sample.

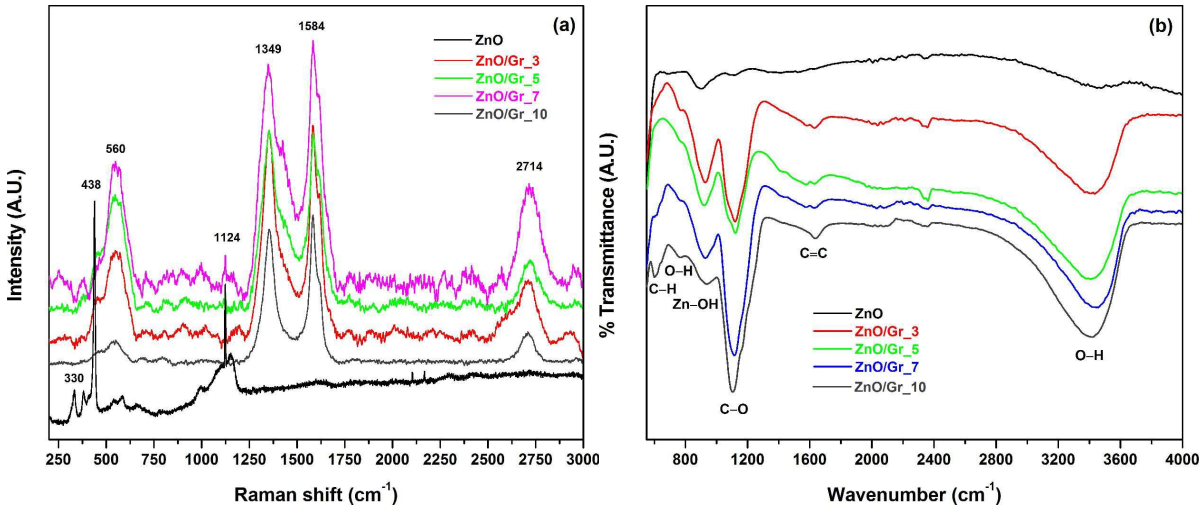

Fig. 3 (a) Raman and (b) ATR-IR spectra of the bare ZnO and ZnO/Gr composites.

A Raman scattering study was performed to confirm the presence of graphene in the composites and shown in Fig. 3a. The Raman spectra of the different ZnO/Gr nanocomposites showed the characteristic peaks for graphene at 1349 (D-band) and 1584 cm^{-1} (G-band), which were assigned to defects or disorder in the graphene and planner configuration of sp^2 bonded carbon structure, respectively.[25] The ZnO/Gr nanocomposites exhibited an intense 2D band at approximately 2714 cm^{-1}. The prepared ZnO/Gr composites also revealed a band at 560 and 1124 cm^{-1}, which was assigned to the longitudinal optical phonon mode with E_1 symmetry (E_1 LO) of oxygen vacancies and with A_1 symmetry (A_1 LO) of the ZnO crystals, respectively. In contrast, peaks corresponding to the second-order vibration mode were also observed at 330 (E_2 low) and 438 cm^{-1} (E_2 high) in the bare ZnO sample.[26] The presence of graphene was clearly depicted in the ATR-IR study of the ZnO/Gr nanocomposites (Fig. 3b). The peaks observed at ~ 1600, 1105 and 602 cm^{-1} in the case of the ZnO/Gr nanocomposites were attributed to the stretching vibration of aromatic C=C, C–O and C–H deformations, respectively.[27] The presence of hydroxyl groups, which were quite high in the case of the ZnO/Gr nanocomposite compared

to bare ZnO due to the in-situ functionalization during synthesis, was identified by the peaks corresponding to the hydrogen bonded –OH groups at ~ 3400 cm^{-1} and O–H bending vibration at 768 cm^{-1}. The weak band at ~ 900 cm^{-1} in the samples was assigned to the Zn–OH vibrations.[28]

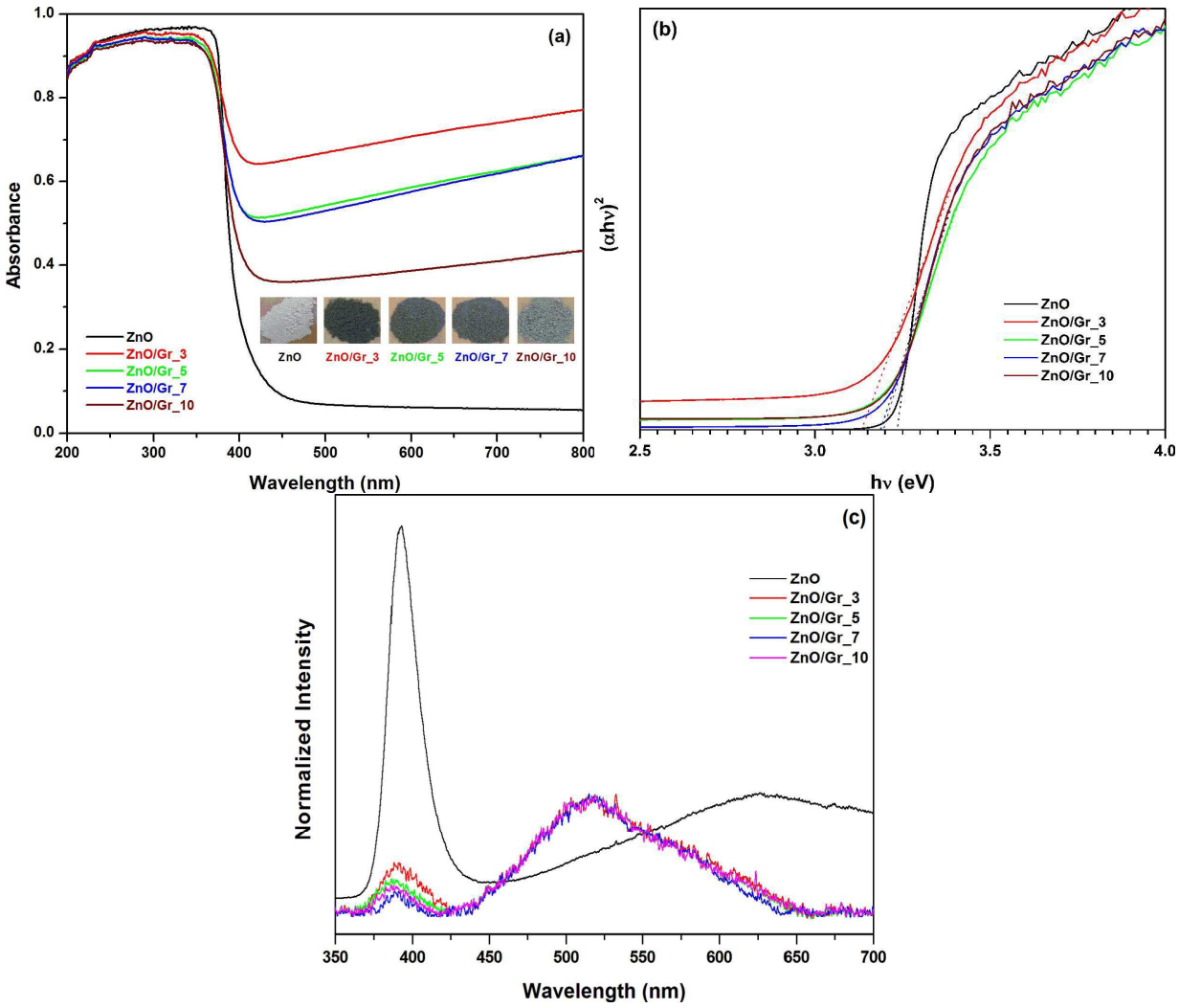

Fig. 4 (a) UV-Vis DRS of bare ZnO and ZnO/Gr nanocomposites, (b) the plot of transformed Kubelka–Munk function as a function of the energy of light and (c) PL spectra of bare ZnO and ZnO/Gr nanocomposites.

The optical properties of the ZnO/Gr nanocomposites were examined by UV-Vis DRS analysis (Fig. 4a). The excitation of an electron from valence to conduction band of ZnO resulted into intense UV light absorption in all samples. The loading of graphene enhances UV light absorption compared to bare ZnO; this enhancement increased with increasing graphene loading. The changes in the ZnO/Gr nanocomposites color (from grayish back to white; inset of Fig. 4a) also supports the decrease in the light absorption capacity with increasing ZnO content. The Kubelka-Munk method was used to determine the band gap of the synthesized composite materials.[29] Fig. 4b shows a plot of $(\alpha h\nu)^2$ (Kubelka-Munk function) vs. hν for different ZnO/Gr nanocomposites. The roughly estimated band gap of ZnO, ZnO/Gr_3, ZnO/Gr_5, ZnO/Gr_7 and ZnO/Gr_10 was 3.23, 3.13, 3.18, 3.19, and 3.20 eV, respectively. The band gap narrowing trend was observed with the introduction of graphene in ZnO, which may be due to the presence of oxygen vacancies and the interfacial interactions between ZnO and graphene.[16]

The PL emission spectrum is widely used to investigate the efficiency of charge carrier trapping, immigration and transfer, and reflect the lifetime of photogenerated electron–hole pairs from semiconductor particles under light illumination. The PL spectra of bare ZnO and ZnO/Gr nanocomposites were recorded at room temperature with excitation wavelength of 325 nm, and displayed in Fig. 4C. The PL spectra of ZnO/Gr nanocomposites contain two emission bands in the UV and visible ranges, which are similar to that of the bare ZnO. The UV emission bands centered at 392 nm and observed in the all samples were resulted from the excitonic recombination, which occurs due to recombination between the electrons in conduction band and the holes in a valence band. The PL intensity of bare ZnO was the highest among all the samples, predicting the high probability of recombination of electrons and holes. The significant decrease in the emission intensity due to graphene incorporation suggesting that, the recombination of

photo-generated carriers was effectively suppressed.[16, 30] Among the all composites, the ZnO/Gr_7 exhibits lowest emission intensity indicating the lower recombination rate of electrons and holes under light irradiation. The incorporation of graphene is mainly responsible for the effective separation of the photogenerated charge carriers and an increased charge carrier lifetime. In particular, graphene is an excellent electron collector and carrier. Thus, the electrons excited from the ZnO particles are transferred to the graphene sheets, which results in a smaller chance of recombining with the generated holes.[31] In addition, an obvious blue-shift of the emission peak of ZnO/Gr nanocomposites observed in the visible region (~ 515 nm) due to the recombination of electrons in a deep defect level or a shallow surface defect level with holes in a valence band was attributed for the presence of oxygen vacancies.[32, 33] It has been found that the presence of oxygen vacancies in the semiconductor can improve its photocatalytic activity.[7, 10] Hence, according to the PL study, synthesized ZnO/Gr nanocomposites are expected to show better photocatalytic activity than bare ZnO.

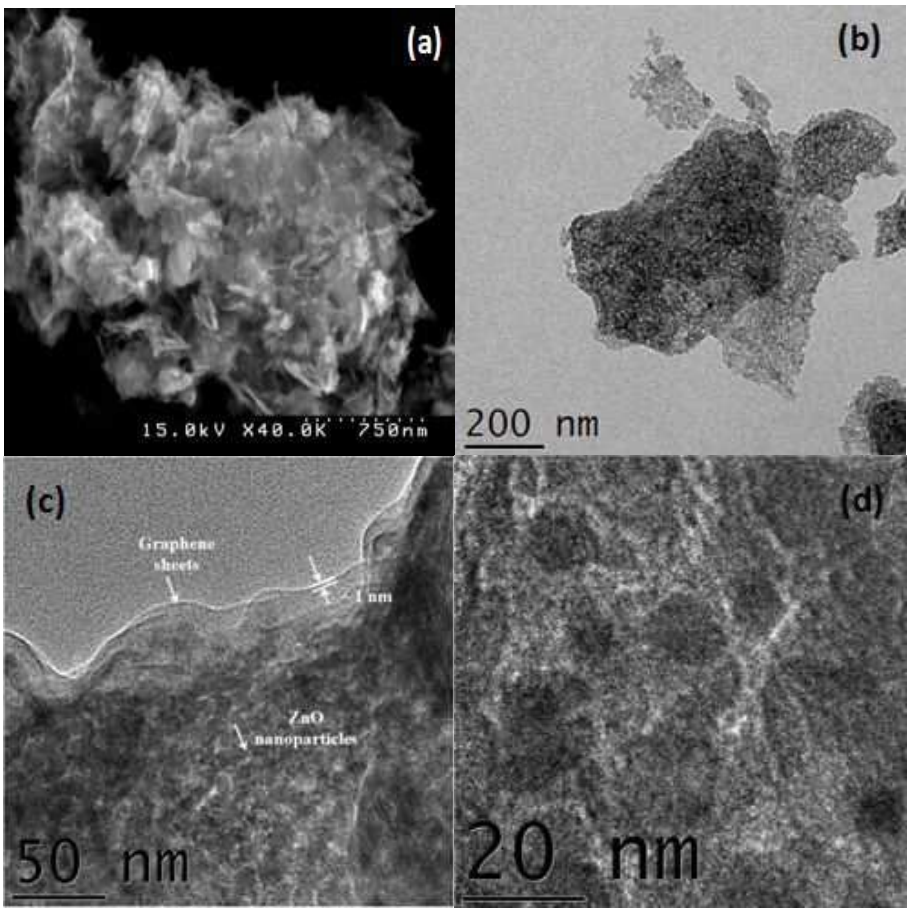

Fig. 5 (a) SEM image showing the ZnO/Gr_7 particle with a sheet structure (b), (c) and (d) TEM images of ZnO/Gr_7 representing the ZnO nanoparticles coating the graphene sheets.

SEM (Fig. 5a) showed that the ZnO/Gr_7 particle had an agglomerated sheet like morphology. The elemental composition of the ZnO/Gr_7 was also determined using EDX assembled with SEM and it was found in accordance with CHN analysis (2.03% C; 72.54% Zn and 25.43% O) (Fig. S1). TEM analysis (Fig. 5b) clearly revealed the uniform decoration of ZnO nanoparticles on the graphene surface, which acts as a two dimensional platform. The graphene sheet thickness measured from the crumpled edges was ~ 1 nm (Fig. 5c), whereas the ZnO particle size was < 20 nm (Fig. 5d). TEM analysis further indicated that the graphene sheets were

fully covered by the ZnO nanoparticles, and no additional free ZnO particles were observed in ZnO/Gr_7. We also carried out the TEM and AFM analysis of the pristine graphene sheets. TEM analysis of the graphene sheets (Fig. S2) clearly depicts its crumpled nature with transparent edges. The crumpling of the graphene sheets is mainly associated with its thermodynamic stability.[34, 35] The lateral size of the graphene sheets was < 1μm. The thickness of the graphene sheets was determined using AFM analysis by casting the graphene/ethanol solution on Si/SiO_2 wafer. Fig. S3 showed the presence of the graphene particles with different shapes and size. Whereas Fig. S4a and S4b showed the section analysis of the two different graphene sheets depicting the thickness of 2.82 and 2.52 nm, respectively which corresponds to its ~ 2-3 layered nature.[23] This result is also supported by the Raman spectrum of the graphene sheets (Fig. S5) showing the intense 2D band at ~ 2690 cm^{-1}.[23] Defect density of the graphitic structure can be determined by measuring the ratio between intensity of D and G band (I_D/I_G ratio), indicating that an increase of the ID /IG ratio means an increase of the defect density in the graphitic structure.[36, 37] From the I_D/I_G ratio, the graphene sheets produced in the present study possesses the higher structural order as compared with the graphene obtained from Hummer's method.[34] The surface area of the prepared samples was determined with nitrogen sorption at 77K. The nitrogen sorption on ZnO/Gr composites exhibited (Fig. 6) Type II physic-sorption isotherm with a H3 type hysteresis loop classified by IUPAC, which are characteristic of the non-porous or macroporous adsorbents.[38] The surface area of the ZnO/Gr nanocomposites increased with increasing graphene loading, and was in the order of bare ZnO (8.50 m^2/g) < ZnO/Gr_10 (26.97 m^2/g) < ZnO/Gr_7 (32.49 m^2/g) < ZnO/Gr_5 (44.29 m^2/g) < ZnO/Gr_3 (48.35 m^2/g).

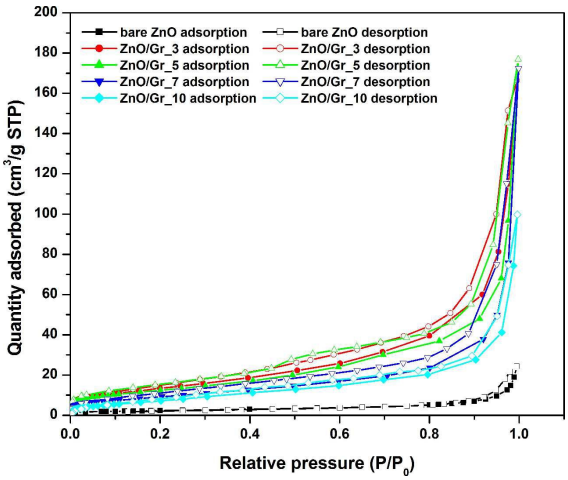

Fig. 6 Nitrogen sorption isotherm of the bare ZnO and ZnO/Gr nanocomposites at 77 K.

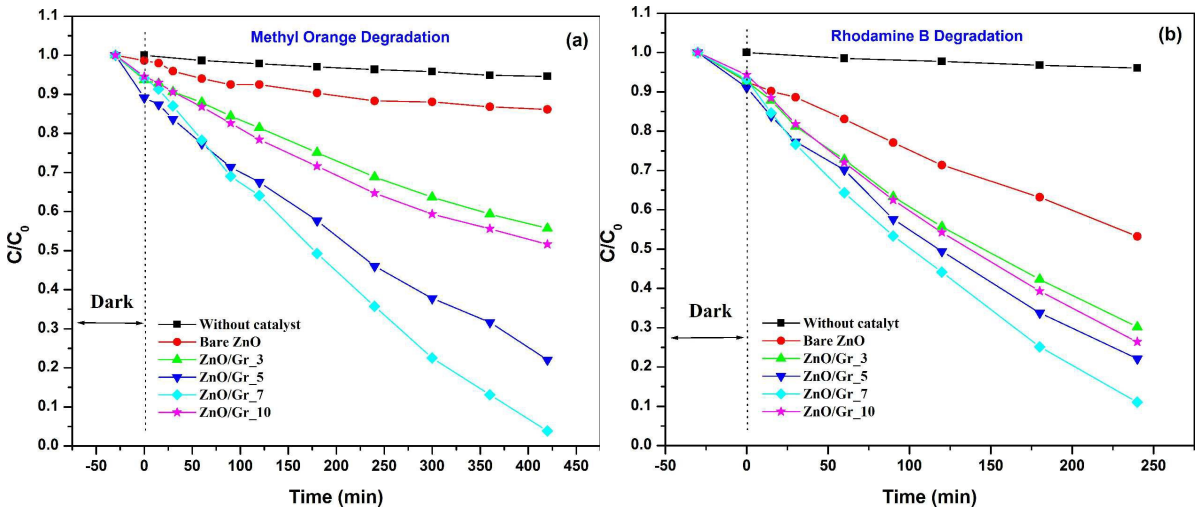

Fig. 7 Photocatalytic degradation of (a) methyl orange and (b) rhodamine B using different ZnO/Gr nanocomposites under UV light.

The photocatalytic activity of the ZnO/Gr nanocomposites and bare ZnO was evaluated from the degradation of Mo (Fig. 7a) and RhB (Fig. 7b) under UV radiation. In both cases, the control experiments, which had been carried out to check the stability of MO and RhB under UV light, revealed the insignificant effect of photolysis (< 5%). The adsorption equilibrium of both

dyes was achieved before the photocatalytic study by stirring the solution in the dark for 30 min. The incorporation of graphene provides more adsorption sites for MO and RhB compared to the bare ZnO due to the π-π conjugation of graphene and dye molecules.[39] As shown in Fig 7a and 7b, among the all prepared ZnO/Gr nanocomposites, ZnO/Gr_7 showed better photocatalytic properties for MO (> 96% in 420 min) and RhB degradation (> 89% in 240 min). Therefore, the graphene loading achieved using a particular reaction condition (i.e. 7 mmol zinc nitrate hexahydrate concentration) was found to be the optimum, and a further increase or decrease in the graphene loading led to a decrease in the photocatalytic activity of the ZnO/Gr nanocomposites (Fig 7a and 7b). The high charge carrier mobility and two dimensional π conjugation structure of graphene improves the separation of electron-hole pairs in semiconductor by doping.[40, 41] In addition, the graphene loading also resulted in improved light absorption capacity of the catalyst, as evidenced by the enhanced light absorption of the photocatalyst with increasing graphene content. These two phenomena were associated mainly with the enhancement in the photocatalytic activity of the ZnO/Gr nanocomposite compared to bare ZnO. The effect of the optimal graphene loading was also observed by the Zhang et al.[41] and Worajittiphon et al.[31] The shielding effect of graphene to the catalytic sites, as well as the light scattering and opacity could decrease the efficiency of photocatalyst with a higher graphene loading.[42-45] The increased concentration of oxygen vacancies with higher graphene loading could also responsible for the decrease in the photoactivity of the catalyst by providing recombination sites for photogenerated charge carriers.[46, 47] As shown in Figs. 7a and 7b, bare ZnO, ZnO/Gr_3, ZnO/Gr_5, ZnO/Gr_7, and ZnO/Gr_10 showed a degradation efficiency of 14, 45, 78, 96, and 48% for MO after 420 min and 47, 70, 78, 89, and 74% for RhB after 240 min, respectively. The above study shows that the optimized and very small graphene loading (1.62

wt.% of C) resulted in a significant enhancement in the photocatalytic activity of the nanocomposite against MO (~7 times) and RhB (~ 2 times). Fig. 8a and 8b shows the decreasing intensities of the UV-Vis absorption spectra for MO and RhB with respect to the irradiation time, whereas their inset depicts the visual color change in the solution due to the decrease in the concentration of MO and RhB, respectively. No new absorption band was observed in the case of MO and RhB, indicating the complete degradation of these dyes. We have also tested ZnO/Gr_7 for its visible light activity for the degradation of MO and RhB with similar catalyst amount (400 mg/L) and dye concentration (10 ppm) using 450 watt visible lamp. ZnO/Gr_7 showed the 13.9 % degradation of MO after 7h and 25.5 % degradation of RhB after 4h as compared with 4.4 and 20.8 % for MO and RhB, respectively using bare ZnO after same time (Fig. S6). Due to the lower catalytic activity of the prepared ZnO/Gr_7 catalyst under visible light, we have further focus on its UV light activity for MO and RhB degradation.

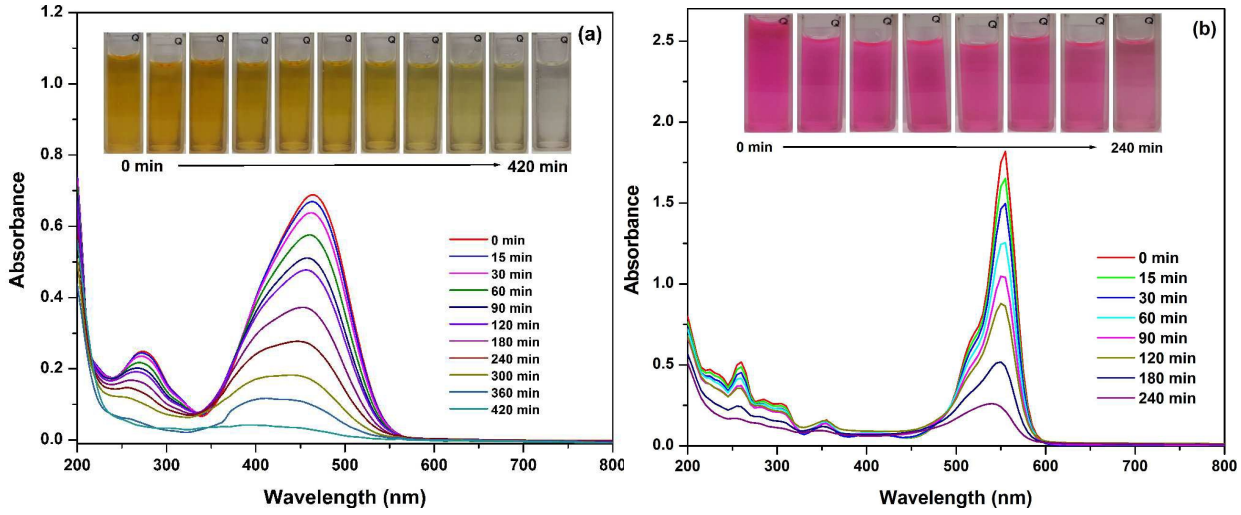

Fig. 8 UV-Vis spectra of (a) MO and (b) RhB after photodegradation at different time intervals using the ZnO/Gr_7 (400 mg/L) catalyst under UV light (The inset shows the change in the color of the dye solution).

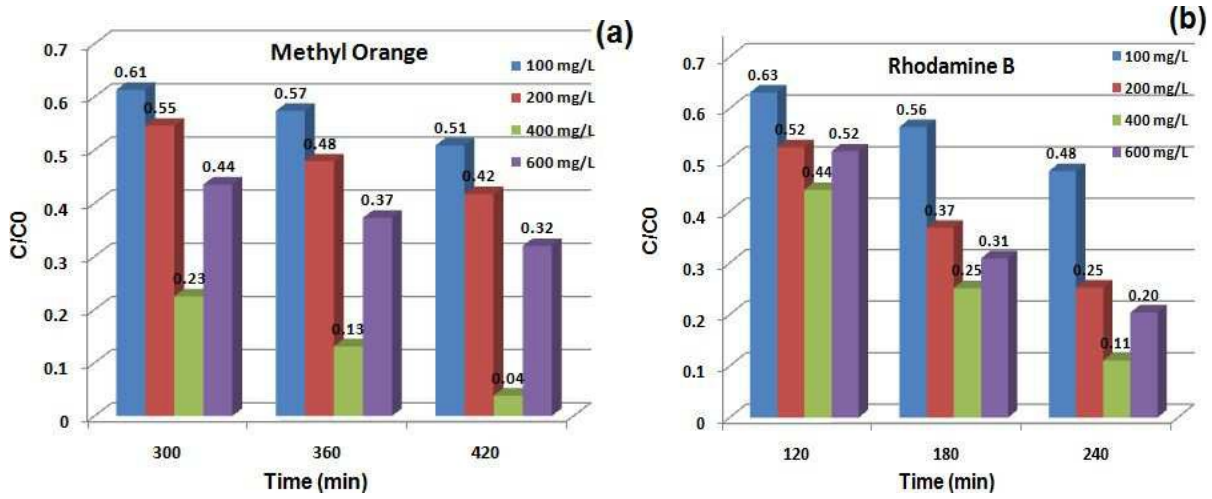

Fig. 9 Effects of ZnO/Gr_7 amount on the photocatalytic degradation of (a) methyl orange and (b) rhodamine B under UV light.

After optimizing the graphene loading, the effects of the catalyst amount on the photocatalytic degradation of MO (Fig. 9a) and RhB (Fig. 9b) was studied under similar conditions using ZnO/Gr_7 as a catalyst. Generally, the photodegradation of dyes increases with increasing the catalyst loading. A similar trend increase photodegradation was found with the ZnO/Gr_7 nanocomposite for photodegradation of MO and RhB with catalyst loading from 100 to 400 mg/L. Further increases in the ZnO/Gr_7 loading i.e. 600 mg/L, resulted in a decrease in the photocatalytic degradation of MO and RhB. A greater catalyst loading (600 mg/L) generated more dense solution which may prevent the penetration of UV light. Therefore, due to the unavailability of the sufficient light intensity, there was a limitation with the electron-hole pair formation, which resulted in a decrease in the photodegradation ability.[39, 42, 48] A 400 mg/L catalyst loading was found to be the optimum with the maximum photodegradation capacity. The photodegradation process of MO and RhB follows pseudo first order kinetics (Fig. S7). Fig.10a presents the rate constant obtained for the different ZnO/Gr nanocomposites. The results showed

that ZnO/Gr_7 possesses the highest rate constant for the MO (0.0066 min^{-1}) and RhB (0.0084 min^{-1}) degradation processes. The prepared ZnO/Gr nanocomposite followed the same order for the rate constant of MO and RhB photodegradation i.e. bare ZnO < ZnO/Gr_3 < ZnO/Gr_10 < ZnO/Gr_5 < ZnO/Gr_7. The reusability of any catalytic system is very important for evaluating its practical uses. The obtained photocatalyst after the photodegradation of MO and RhB was collected and washed with sufficient water and methanol followed by drying at 150 ºC for 5 h. The obtained catalyst was treated further with a fresh MO or RhB solution to evaluate its recycling ability. As shown in Fig. 10b, the ZnO/Gr_7 possesses an efficient recycling ability up to four runs or even more with < 12% loss of photocatalytic ability.

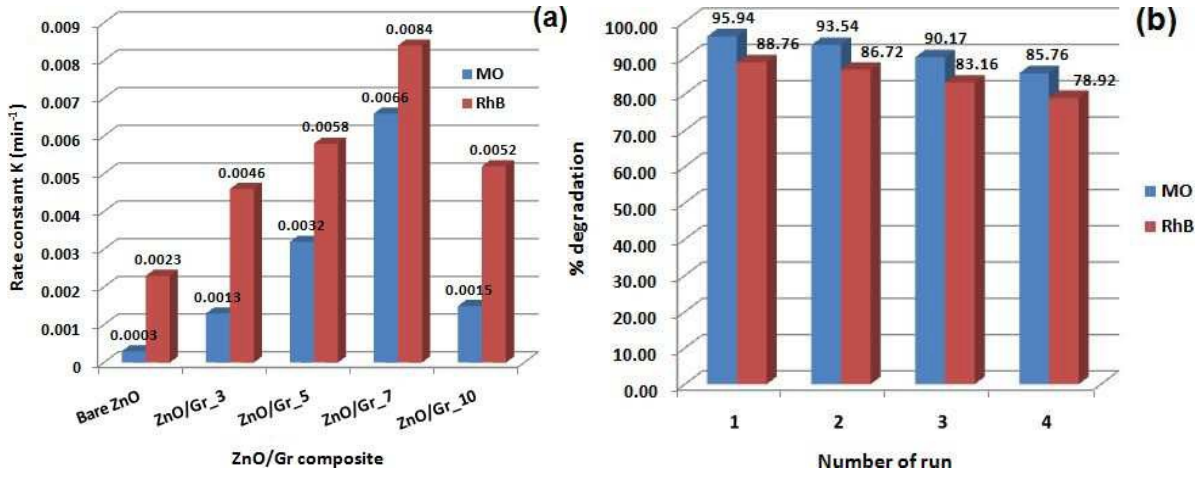

Fig. 10 (a) Pseudo-first order rate constant for the degradation of methyl orange and rhodamine B using bare ZnO and different ZnO/Gr nanocomposites (300 mg/L) and (b) recycling study of ZnO/Gr_7 for MO and RhB photodegradation under UV light.

Fig. 11 Schematic diagram of proposed mechanism for the photodegradation of dyes over the ZnO/Gr nanocomposite under UV light.

Fig. 11 presents the possible mechanism for photocatalytic degradation of pollutant (MO and RhB) by ZnO/Gr composites. By adsorbing energy from UV radiation, the electrons from the valence band of ZnO excited to the conduction band leaving behind a hole. The recombination of excited electron follow the graphene intermediate path instead of direct transfer to the hole due to the intermediate work function of graphene (-4.42 eV) compared to valence (-7.25 eV) and conduction (-4.05 eV) bands of ZnO.[20, 49] This extended charge separation process effectively reduces the likelihood of the recombination of newly generated electrons and holes, and significantly increases the lifespan of the holes in the ZnO/Gr composite.[50] The generated electrons and holes react with dissolved oxygen and water (or hydroxyl groups), respectively, producing reactive free radicals, which are responsible for the oxidation of the dye molecules to CO_2, H_2O and other mineralized intermediates.[51]

The synthesis of ZnO/GO and ZnO/rGO (2 wt% each) were also performed using KOH precipitation method in which GO was prepared using modified Hummer's method[52] and rGO

using modified Wallace's method.[53, 54] The obtained catalysts were characterized using XRD (Fig. S8) and confirmed the formation of ZnO before testing their photocatalytic performance. In case of both catalysts, the degradation of MO and RhB were found lower as compare with the ZnO/Gr_7 under similar experimental conditions and not much difference with each other. ZnO/GO and ZnO/rGO showed the 27 and 30% MO degradation and 55 and 60% RhB degradation under similar conditions. It is worth noting that the graphene produced using the electrochemical exfoliation possesses less defects with superior electrical properties compared with commonly used reduced graphene oxide, which preparation typically requires many steps including oxidation of graphite and high temperature reduction.[22, 23] As shown in the Raman analysis (Fig. S5), the graphene prepared in the present study carries less defects as compared with the GO prepared using Hummer's method and rGO. Hence, the ZnO/Gr nanocomposite obtained in the present study contains less defective graphene and resulted in the higher photodegradation activity for MO and RhB over ZnO/GO and ZnO/rGO photocatalyst prepared using commonly used Hummer's method. Table 1 showed the comparison of the different ZnO/Gr photocatalyst prepared using various graphene synthesis methodologies for the degradation of MO and RhB under UV radiation. With detail understanding of the previously reported work based on the ZnO/Gr photocatalysts, we comes to know that it possesses their own advantages over each other compare with photocatalytic ability, ease of preparation, stability and morphologies. Notably, the results shown in Table 1 could not be comparable due to the variation in other experimental conditions such as power of light source, distance from light source, preparation methodology, etc. The present work possesses the advantage of *in-situ* synthesis of few layered less defective graphene/ZnO composite with enhanced photocatalytic activity.

Table 1 Recent studies on the degradation of RhB and MO using ZnO/Gr based photocatalyst under UV light

Catalyst	Dye	Dye Conc. (ppm)	Catalyst amount (mg/L)	Time (min)	Degradation (%)	UV light Power (watt)	Graphene synthesis method	References
ZnO/Gr	RhB	10	1250	60	~100	15	Modified Hummer's method	Zhang et al.[26]
ZnO/rGO	RhB	4.8	1000	20	89	500	Modified Hummer's method	Yao et al.[33]
ZnO/Amine functionalized Gr	RhB	7.5	500	40	98	18	Commercial sample	Worajittiphon et al.[31]
ZnO/rGO	RhB	10	250	120	~100	300	Modified Hummer's method	Weng et al.[40]
ZnO/Gr	RhB	10	1000	20	~100	300	Hummer's method	Bu et al.[55]
ZnO/Gr	RhB	15	500	25	~60	350	Modified Hummer's method	Saravanakumar et al.[56]
ZnO/Gr	RhB	10	400	240	89	16	Electrochemical exfoliation	Present study
ZnO/N-doped Gr	MO	10	750	15	~95	300	Hummer's and Offeman method	Liu et al.[57]
ZnO/Gr	MO	5	400	200	~100	175	Supercritical CO_2 assisted with ultrasound	Leng et al.[18]

ZnO/rGO	MO	10	450	90	78	250	Hummer's and Offeman method	Nipane et al.[58]
ZnO/Gr	MO	10	800	90	> 95	300	Modified Hummer's method	Yin et al.[59]
ZnO/rGO	MO	40	100	150	~100	100	Modified Staudenmaier method	He et al.[60]
ZnO/Gr	MO	10	400	420	96	16	Electrochemical exfoliation	Present study

4. Conclusion

A series of ZnO/Gr nanocomposites were synthesized by the electrochemical assisted synthesis of graphene followed by precipitation using a basic medium and calcination process. The graphene loading was varied using different concentrations of zinc precursor as an electrolyte in combination with sulfuric acid. The present methodology allows the efficient and facile synthesis of ZnO nanoparticles-decorated graphene sheets in high yield, as examined by SEM and TEM. The amount of graphene is a crucial factor and affects the photocatalytic activity of the composite. The ZnO/Gr nanocomposite prepared with 7 mmol zinc nitrate showed enhanced photodegradation ability for MO (~ 7 times) and RhB (~ 2 times) compared to bare ZnO under UV light. The ZnO/Gr nanocomposite with less defective graphene sheets produced *in-situ* using electrochemical exfoliation showed enhanced photocatalytic performance as compared with commonly used GO and rGO. The reported work shows a new methodology for the synthesis of ZnO/Gr nanocomposites as an efficient and recyclable photocatalyst for pollutant remediation.

Acknowledgements

This study was supported by Priority Research Centers Program (Grant No: 2014R1A6A1031189), and Basic Science Research Program (Grant No: 2015R1D1A3A03018029) through the National Research Foundation of Korea (NRF) funded by the Ministry of Education.

References

1. P. V. L. Reddy and K.-H. Kim, *J. Hazard. Mater.*, 2015, **285**, 325-335.

2. S. G. Kumar and L. G. Devi, *J. Phys. Chem. A*, 2011, **115**, 13211-13241.

3. K. Kabra, R. Chaudhary and R. L. Sawhney, *Ind. Eng. Chem. Res.*, 2004, **43**, 7683-7696.

4. A. A. Ismail and D. W. Bahnemann, *Sol. Energ. Mat. Sol. C*, 2014, **128**, 85-101.

5. L. J. Liu and Y. Li, *Aerosol Air Qual. Res.*, 2014, **14**, 453-469.

6. C. Minero, G. Mariella, V. Maurino, D. Vione and E. Pelizzetti, *Langmuir*, 2000, **16**, 8964-8972.

7. S. A. Ansari, M. M. Khan, S. Kalathil, A. Nisar, J. Lee and M. H. Cho, *Nanoscale*, 2013, **5**, 9238-9246.

8. S. A. Ansari, M. M. Khan, M. O. Ansari, J. Lee and M. H. Cho, *.J. Phys. Chem. C*, 2013, **117**, 27023-27030.

9. T. Natarajan, K. Natarajan, H. Bajaj and R. Tayade, *J. Nanopart. Res.*, 2013, **15**, 1-18.

10. M. M. Khan, S. A. Ansari, D. Pradhan, M. O. Ansari, D. H. Han, J. Lee and M. H. Cho, *J. Mater. Chem. A*, 2014, **2**, 637-644.

11. V. Apostolopoulou, J. Vakros, C. Kordulis and A. Lycourghiotis, *Colloid Surface A*, 2009, **349**, 189-194.

12. S. Wang and S. Zhou, *J. Hazard. Mater.*, 2011, **185**, 77-85.

13. W.-K. Jo, Y. Won, I. Hwang and R. J. Tayade, *Ind. Eng. Chem. Res.*, 2014, **53**, 3455-3461.

14. R. K. Upadhyay, N. Soin and S. S. Roy, *Rsc. Adv.*, 2014, **4**, 3823-3851.

15. J. Wang, H. M. Huang, Z. Z. Xu, J. H. Kou and C. H. Lu, *Curr. Org. Chem.*, 2014, **18**, 1346-1364.

16. Z. Chen, N. Zhang and Y. J. Xu, *Crystengcomm*, 2013, **15**, 3022-3030.

17. X. Zhou, T. J. Shi and H. O. Zhou, *Appl. Surf. Sci.*, 2012, **258**, 6204-6211.

18. Y. P. Leng, W. C. Wang, L. Zhang, F. Zabihi and Y. P. Zhao, *J. Supercrit. Fluid*, 2014, **91**, 61-67.

19. J. A. Lin, M. Penchev, G. P. Wang, R. K. Paul, J. B. Zhong, X. Y. Jing, M. Ozkan and C. S. Ozkan, *Small*, 2010, **6**, 2448-2452.

20. A. Wei, L. Xiong, L. Sun, Y. J. Liu, W. W. Li, W. Y. Lai, X. M. Liu, L. H. Wang, W. Huang and X. C. Dong, *Mater. Res. Bull.*, 2013, **48**, 2855-2860.

21. Y. C. Gong, C. W. Zou, Y. D. Yao, W. D. Fu, M. Wang, G. F. Yin, Z. B. Huang, X. M. Liao and X. C. Chen, *J. Mater. Sci.*, 2014, **49**, 5658-5666.

22. C. T. J. Low, F. C. Walsh, M. H. Chakrabarti, M. A. Hashim and M. A. Hussain, *Carbon*, 2013, **54**, 1-21.

23. C.-Y. Su, A.-Y. Lu, Y. Xu, F.-R. Chen, A. N. Khlobystov and L.-J. Li, *Acs Nano*, 2011, **5**, 2332-2339.

24. A. Sinhamahapatra, A. K. Giri, P. Pal, S. K. Pahari, H. C. Bajaj and A. B. Panda, *J. Mater. Chem.*, 2012, **22**, 17227-17235.

25. S. Y. Sawant, R. S. Somani, S. S. Sharma and H. C. Bajaj, *Carbon*, 2014, **68**, 210-220.

26. Q. Zhang, C. G. Tian, A. P. Wu, T. X. Tan, L. Sun, L. Wang and H. G. Fu, *J. Mater. Chem.*, 2012, **22**, 11778-11784.

27. S. Y. Sawant, R. S. Somani and H. C. Bajaj, *Carbon*, 2010, **48**, 668-672.

28. A. Kolodziejczak-Radzimska, E. Markiewicz and T. Jesionowski, *J. Nanomater.*, 2012, Doi 10.1155/2012/656353.

29. R. López and R. Gómez, *J. Sol-Gel Sci. Techn.*, 2012, **61**, 1-7.

30. D. L. Li, W. H. Wu, Y. P. Zhang, L. L. Liu and C. X. Pan, *J. Mater. Sci.*, 2014, **49**, 1854-1860.

31. P. Worajittiphon, K. Pingmuang, B. Inceesungvorn, N. Wetchakun and S. Phanichphant, *Ceram. Int.*, 2015, **41**, 1885-1889.

32. G. R. Li, T. Hu, G. L. Pan, T. Y. Yan, X. P. Gao and H. Y. Zhu, *J. Phys. Chem. C*, 2008, **112**, 11859-11864.

33. C. L. Yao, A. J. Xie, Y. H. Shen, W. N. Zhu and J. M. Zhu, *Cryst. Res. Technol.*, 2014, **49**, 982-989.

34. M. Alanyalioglu, J. J. Segura, J. Oro-Sole and N. Casan-Pastor, *Carbon*, 2012, **50**, 142-152.

35. S. Y. Sawant, R. S. Somani, M. H. Cho and H. C. Bajaj, *Rsc Adv.*, 2015, **5**, 46589-46597.

36. G. Wang, B. Wang, J. Park, Y. Wang, B. Sun and J. Yao, *Carbon*, 2009, **47**, 3242-3246.

37. A. C. Ferrari and J. Robertson, *Phys. Rev. B*, 2000, **61**, 14095-14107.

38. F. Rouquerol, J. Rouquerol and K. Sing, in *Adsorption by Powders and Porous Solids*, eds. F. Rouquerol, J. Rouquerol and K. Sing, Academic Press, London, 1999, DOI: http://dx.doi.org/10.1016/B978-012598920-6/50002-6, pp. 1-26.

39. Y. Zhang, Z.-R. Tang, X. Fu and Y.-J. Xu, *Acs Nano*, 2010, **4**, 7303-7314.

40. B. Weng, M. Q. Yang, N. Zhang and Y. J. Xu, *J. Mater. Chem. A*, 2014, **2**, 9380-9389.

41. Y. H. Zhang, Z. Chen, S. Q. Liu and Y. J. Xu, *Appl. Catal. B*, 2013, **140**, 598-607.

42. Y. Zhang, N. Zhang, Z.-R. Tang and Y.-J. Xu, *Acs Nano*, 2012, **6**, 9777-9789.

43. Q. Li, B. Guo, J. Yu, J. Ran, B. Zhang, H. Yan and J. R. Gong, *J. Am. Chem. Soc.*, 2011, **133**, 10878-10884.

44. Q. Xiang and J. Yu, *J. Phys. Chem. Lett.*, 2013, **4**, 753-759.

45. Q. Xiang, J. Yu and M. Jaroniec, *J. Phys. Chem. C*, 2011, **115**, 7355-7363.

46. X. Pan, N. Zhang, X. Fu and Y.-J. Xu, *Appl. Catal. A*, 2013, **453**, 181-187.

47. X. Pan, M.-Q. Yang, X. Fu, N. Zhang and Y.-J. Xu, *Nanoscale*, 2013, **5**, 3601-3614.

48. Y. Zhang, Z.-R. Tang, X. Fu and Y.-J. Xu, *Acs Nano*, 2011, **5**, 7426-7435.

49. V. Srikant and D. R. Clarke, *J. Appl. Phys.*, 1998, **83**, 5447-5451.

50. L. Zhang, L. H. Du, X. Cai, X. Yu, D. D. Zhang, L. C. Liang, P. H. Yang, X. B. Xing, W. J. Mai, S. Z. Tan, Y. Gu and J. H. Song, *Physica E*, 2013, **47**, 279-284.

51. W. J. Ong, S. Y. Voon, L. L. Tan, B. T. Goh, S. T. Yong and S. P. Chai, *Ind. Eng. Chem. Res.*, 2014, **53**, 17333-17344.

52. W. S. Hummers and R. E. Offeman, *J. Am. Chem. Soc.*, 1958, **80**, 1339-1339.

53. Y. Gao, D. Ma, C. Wang, J. Guan and X. Bao, *Chem. Commun.*, 2011, **47**, 2432-2434.

54. D. Li, M. B. Muller, S. Gilje, R. B. Kaner and G. G. Wallace, *Nat. Nanotechnol.*, 2008, **3**, 101-105.

55. Y. Y. Bu, Z. Y. Chen, W. B. Li and B. R. Hou, *Acs Appl. Mater. Inter.*, 2013, **5**, 12361-12368.

56. B. Saravanakumar, R. Mohan and S.-J. Kim, *Mater. Res. Bull.*, 2013, **48**, 878-883.

57. L. Liu, C. Dong, K.-L. Wu, Y. Ye and X.-W. Wei, *Mater. Lett.*, 2014, **129**, 170-173.

58. S. V. Nipane, P. V. Korake and G. S. Gokavi, *Ceram. Int.*, 2015, **41**, 4549-4557.

59. D. Yin, L. Zhang, B. Liu and M. Wu, *J. Nanosci. Nanotechnol.*, 2012, **12**, 937-942.

60. J. He, C. Niu, C. Yang, J. Wang and X. Su, *Rsc Adv.*, 2014, **4**, 60253-60259.

Graphical abstract: